https://doi.org/10.5194/angeo-2024-3
Preprint. Discussion started: 23 April 2024

Annales Geophysicae Discussions
Open Access
EGU

Impact of solar cycle on the non-linearity of the relationship between the solar wind parameters and geomagnetic conditions

Hoilijoki Sanni[1], Kilpua Emilia[1], Osmane Adnane[1], Turc Lucile[1], Savola Mikko[1], Lipsanen Veera[1], George Harriet[2], and Kalliokoski Milla[3]

[1]Department of Physics, University of Helsinki, Helsinki, Finland
[2]Laboratory for Atmospheric and Space Physics, University of Colorado, Boulder, USA
[3]Institute of Space and Astronautical Science, Japan Aerospace Exploration Agency, Sagamihara, Japan

Correspondence: Sanni Hoilijoki (sanni.hoilijoki@helsinki.fi)

Abstract. Solar wind and its transients drive the dynamics of Earth's magnetosphere. Interplanetary coronal mass ejections (ICMEs) induce the largest variations in the near-Earth space, but significant geomagnetic activity can also be driven by high-speed streams (HSSs) and stream interaction regions (SIRs). Solar wind – magnetosphere interaction may lead to fluctuations in the inner magnetosphere and, hence, impact the electrons in the outer radiation belt. In this study, we use mutual information from information theory to study the change in the statistical dependence between solar wind parameters and inner magnetospheric indices including ultra low frequency (ULF) waves in the Pc5 range and electrons in the outer radiation belt during solar cycle 23 (1998-2008). Unlike Pearson correlation coefficient, mutual information can be used to investigate non-linear statistical dependencies between different parameters. We calculate linear and non-linear correlation coefficients separately for each year during solar cycle 23 and define the non-linearity with the ratio between the linear and non-linear correlation coefficients. We find that the non-linearity between solar wind speed and electron flux index is higher during solar maximum when most of the geomagnetic activity is driven by ICMEs, while the non-linearity decreases during the declining phase, when a larger portion of the geomagnetic activity is driven by HSSs and SIRs. On the other hand, IMF B_z and solar wind electric field $E_y = V_{sw}B_z$ have smaller non-linearity with the geomagnetic indices during time periods of stronger geomagnetic activity.

To investigate further if the change of the ratio of ICMEs and SIRs/HSSs as the driver of geomagnetic activity is the possible cause of the changes in the non-linearity during the solar cycle, we calculate the correlation coefficients separately during ICMEs, HSSs/SIRs and quiet solar wind. We find that non-linearity for solar wind speed and inner magnetospheric electron flux and ULF wave indices is smallest and correlations (both linear and non-linear) highest and therefore, the non-linearity is the lowest during the quiet time, while other studied solar wind parameters correlate better either during HSSs or ICMEs. These results show that the selected time period (phase of the solar cycle, dominant driver of the geomagnetic activity during the selected time) for the correlation analysis can significantly impact the results. Results also indicate that during ICMEs the solar wind – magnetosphere coupling becomes more non-linear for the majority of the studied solar wind–magnetospheric index parameter pairs (velocity, density, dynamic pressure) but IMF B_z and solar wind electric field $E_y = V_{sw}B_z$ have smaller non-linearity during time periods of stronger geomagnetic activity.

https://doi.org/10.5194/angeo-2024-3
Preprint. Discussion started: 23 April 2024

Annales Geophysicae Discussions

1 Introduction

The solar wind is the driver of geomagnetic activity in the Earth's magnetosphere (e.g., Pulkkinen, 2007; Kilpua et al., 2017b). The strongest geomagnetic disturbances occur during interplanetary coronal mass ejections (ICMEs) (e.g. Richardson, Ian G. and Cane, Hilary V., 2012; Kilpua et al., 2017a) that are the interplanetary counterparts of massive eruptions of magnetized plasma from the Sun. Geomagnetic activity also occurs during high speed streams (HSSs) originating from coronal holes and during the stream interaction regions (SIRs) of piled-up plasma and magnetic field HSSs form when interacting with the slower wind ahead (Sheeley et al., 1976; Richardson, 2018). HSSs/SIRs cause mainly weak and moderate geomagnetic storms (Tsurutani et al., 2006; Borovsky and Denton, 2006). During and near the solar maxima the ICMEs are the most frequent, fastest and have the strongest magnetic fields, and thus, dominate the geomagnetic disturbances (e.g. Richardson, Ian G. and Cane, Hilary V., 2012). In the late declining phase and during solar minimum the number of ICMEs decreases, in particular strong and fast ones, and HSSs/SIRs become the main cause of geomagnetic storms (Gonzalez et al., 1999; Tsurutani et al., 2006). ICMEs passage time last typically 1 day (e.g., Kilpua et al., 2017a), while the HSSs can last for multiple days. HSSs and hence SIRs may be recurrent with 27 day periods as the coronal holes that are the sources of the fast wind may exist for multiple solar rotations. Therefore, SIRs are also called co-rotating interaction regions (CIRs).

During geomagnetic storms the magnetospheric and ionospheric current systems intensify and change rapidly (e.g Gonzalez et al., 1994; Borovsky and Denton, 2006), and high energy particle fluxes and plasma wave activity are enhanced inside the magnetosphere. Substorms are a global phenomena in the magnetosphere where energy from the solar wind accumulates in the magnetotail and then unloads in a few hour periods (e.g McPherron, 1979). During substorms magnetic reconnection in the Earth's magnetotail injects electrons from the plasma sheet towards the inner magnetosphere accelerating them from a few keV to a few hundred keVs. These electrons can get trapped in the Earth's magnetic field forming the outer radiation belt. Their interactions with different wave modes may accelerate them up to relativistic (MeV) energies.

An important class of waves for the electron dynamics in the inner magnetosphere are ultra low frequency (ULF) waves (e.g., Elkington et al., 2003; Shprits et al., 2008; Mann et al., 2013, 2016). ULF oscillations in the Earth's magnetic field especially in the Pc5 range (2-7 mHz) can drift resonate with energetic radiation belt electrons (e.g., Elkington et al., 1999; Elkington et al., 2003) and in the case of large-amplitude, lead to fast and nonlinear radial transport (Osmane et al., 2023). The magnetospheric ULF waves are regularly recorded both from spacecraft observations and from ground-based magnetometers(e.g., Bentley et al., 2018; Sarris et al., 2022). ULF waves can be divided to toroidal (azimuthal magnetic field and radial electric field), poloidal (radial magentic field and azimuthal electric field) and compressional (field aligned magnetic field and azimuthal electric field) modes. The toroidal components are usually observed with large extent in the azimuthal direction (small wave number m) and they have been found to be driven by external sources i.e. direct driving by the solar wind (e.g. dynamic pressure pulses, Kelvin-Helmholtz instability driven by the velocity shear, reconnection and formation and propagation of flux transfer events at the dayside magnetopause) (e.g. Hudson et al., 2004; Claudepierre et al., 2008). Poloidal modes have shorter azimuthal extent and they have been found to be driven by internal sources for example, generation via magnetospheric processes such as bounce-drift resonance and other wave-particle interactions (e.g. Southwood et al., 1969). Nevertheless, the ultimate source for

https://doi.org/10.5194/angeo-2024-3
Preprint. Discussion started: 23 April 2024

Annales Geophysicae Discussions

the internal driving is also in the solar wind that drives the geomagnetic activity. The ULF waves measured in space (typically at the geosynchronous orbit) may be composed of toroidal, poloidal and compressional components. However, ULF Pc5 wave activity measured in space and on ground do not necessarily have one-to-one correlation. Toroidal modes propagate along the magnetic field lines and they are often measured by the ground magnetometers. Poloidal waves, on the other hand, are rarely observed on the ground due to iononospheric screening effect (Hughes and Southwood, 1976) but there are also studies reporting long lasting occurrences of poloidal ULF waves seen in the ground magnetometers Shi et al. (2018).

The key external driver of ULF waves is the solar wind velocity (e.g. Mathie and Mann, 2001; Bentley et al., 2018). The ULF wave activity in the inner magnetosphere is known to increase during higher solar wind speeds because that increases the occurrence of Kelvin-Helmholtz instability at the flanks of the magnetopause. In addition, solar wind speed has been shown to be the dominant driver of the electron fluxes over all energies in the outer radiation belt with increasing time lag for higher energy electrons (e.g. Paulikas and Blake, 1979; Baker et al., 1990; Li et al., 2005; Reeves et al., 2011; Wing et al., 2016, 2021). This correlation, between speed and high energy electron fluxes likely stems both from the increased ULF wave activity enhancing the transport and subsequent acceleration of electrons and the increased substorm activity injecting more frequently source energy electrons (few tens of keV) to be accelerated. This complex and interlinked driving is expected to give non-linear correlations between the solar wind parameters, ULF waves and their effects to electrons (e.g., March et al., 2005; Johnson and Wing, 2005; Reeves et al., 2011; Kellerman and Shprits, 2012; Wing et al., 2016, 2021; Osmane et al., 2022; Simms et al., 2021; Hoilijoki et al., 2022).

Previous studies have also indicated clear differences in the non-linearities in the magnetospheric response to solar wind in different solar cycle phases (e.g., Johnson and Wing, 2005; Hoilijoki et al., 2022). For example, the results by Hoilijoki et al. (2022) indicated that the non-linearity between the AE index and electron precipitation at different MLT sectors was higher for the solar maximum year 2004 than for the solar minimum year 2007. This difference is likely due to the different contribution from ICMEs and SIR/HSS driven storms and the subsequent differences in the dominant driving conditions and the level of geomagnetic activity suggesting that the solar wind–magnetosphere coupling becomes more non-linear during ICME driven geomagnetic activity. Johnson and Wing (2005) studied the changes in non-linear dependence of solar wind–magnetosphere coupling during multiple solar cycle. They concluded that the non-linearities in the Kp index and solar wind driving with VB_S (where B_S is the southward component of the IMF) is more linear during solar maximum. In this paper, we investigate the non-linearity of the solar wind–magnetosphere coupling using mutual information. We use five different solar wind parameters, AE and SYM-h indices, geosynchronous and ground based Pc5 ULF waves indices and radiation belt electron flux index. We find that for majority of solar wind drivers, especially for solar wind speed, the non-linearity is larger during solar maximum and smaller during the minimum. The paper is organized as follows: Data and methods used in this study are described in Section 2 and the results are shown in Section 3. The results are discussed and concluded in Sections 4 and 5, respectively.

https://doi.org/10.5194/angeo-2024-3
Preprint. Discussion started: 23 April 2024

Annales Geophysicae Discussions

2 Data and Methods

2.1 Data and indices

In this study we use solar wind parameters and geomagnetic indices, AE and SYM-H, obtained from NASA's OMNI data (https://omniweb.gsfc.nasa.gov/index.html). The start and end times of the ICMEs are obtained from the Richardson and Cane ICME catalogue (https://izw1.caltech.edu/ACE/ASC/DATA/level3/icmetable2.htm) (Richardson and Cane, 2024) and the times for the SIRs and HSSs are from the list combined by Grandin et al. (2019). In this list, the time periods are listed as SIR/HSS if the time derivative of B at the leading edge is above the threshold 0.6 nT/h, the preceding solar wind speed is less than 450 km/s, the solar wind speed increases at least 30 km/s/day and the velocity reaches 500 km/s or more within three days of the start of the SIR.

ULF wave indices used in this study, T_{geo} and T_{gr}, are 1 h resolution measurements of the total spectral power of the magnetic field fluctuations from geosynchronous and ground-based observations, respectively, in the 2-7 mHz frequency band obtained from the data archive: https://doi.org/10.2205/ULF-index (Kozyreva et al., 2007; Pilipenko et al., 2017b). The ground based ULF wave index T_{gr} is obtained ground-based magnetometers at 60°-70° latitude from the Northern hemisphere between MLTs 03 and 18 using the two horizontal magnetic field components (Kozyreva et al., 2007; Pilipenko et al., 2017b). The threshold parameter for the ground-based ULF wave index is set so that only one station with the highest ULF power is selected for each time interval. The geosynchronous T_{geo} is calculated using the data from GOES spacecraft that are located on the geosynchronous orbit at 6.6 R_E on the equatorial plane. T_{geo} is calculated using all three components of the magnetic field as a sum of the spectral power of each component and, therefore, the T_{geo} includes all components of the ULF Pc5 waves (toroidal, poloidal and compressional). In this study we use the indices as logarithm in base 10 of the total spectral power.

To correlate the solar wind parameters with the outer radiation belt electron fluxes, we use the electron flux index derived by Borovsky and Yakymenko (2017). F_{e130} describes electrons near 130 keV in the outer magnetosphere. Electrons at these energies are in particular interest because they can drive the whistler mode chorus waves. Electrons injected from the magnetotail during substorms around 130 keV are found to serve as source electrons for radiation belt energetic electrons. The measurements for the index are made using synchronous orbit particle analyzer (SOPA) energetic particle instrument on board the Los Alamos National Laboratory (LANL) spacecraft. On each spacecraft the 10 s resolution data is used to calculate 6 min median values for the given energy channels. For each hour of universal time, the maximum of the 6 minute median values from all spacecraft is chosen and the index F_{e130} is defined as the 10 base logarithm of the maximum.

2.2 Mutual information

Mutual information (MI) from information theory can be used to study non-linear statistical dependencies between two parameters (e.g. Li, 1990; Cover and Thomas, 2006). This makes it distinct from e.g. the widely used Pearson correlation coefficient that only measures the linear correlation. MI quantifies the amount of shared information in two random variables X and Y. The method applied in this study is described more in detail by Osmane et al. (2022) and also used in the study by Hoilijoki et al. (2022) but below we describe the main points of the MI. Entropy, H, is a measure of the uncertainty that for variables X

https://doi.org/10.5194/angeo-2024-3
Preprint. Discussion started: 23 April 2024

Annales Geophysicae Discussions Open Access EGU

and Y can be written as:

$$H(X) = -\sum_{x \in X} p(x) \log p(x); \qquad H(Y) = -\sum_{y \in Y} p(y) \log p(y) \tag{1}$$

where $p(x)$ and $p(y)$ are the probability mass functions of variables X and Y, respectively. The joint entropy between variables X and Y takes the form:

$$H(X,Y) = -\sum_{x,y} p(x,y) \log \left(p(x,y) \right), \tag{2}$$

where $p(x,y)$ is the joint probability mass function of X and Y. By definition, MI reveals how much information we can know about one variable just by measuring the other. Therefore, MI can be written as an uncertainty of measuring variables X and Y separately compared to measuring them together:

$$MI(X,Y) = H(X) + H(Y) - H(X,Y) = \sum_{y \in Y} \sum_{x \in X} p(x,y) \log_2 \left(\frac{p(x,y)}{p(x)p(y)} \right). \tag{3}$$

To compare the linear Pearson correlation coefficient and MI, we calculate the information adjusted correlation, ρ_{adj} (Osmane et al., 2022). This parameter is defined using the following reasoning. It is assumed that the analyzed variables X and Y are Gaussian bivariate distributed. In this case the MI and linear correlation are exact and related through the equation

$$\mathrm{MI} = -\frac{1}{2} \log(1 - \rho^2), \tag{4}$$

from where the estimated information adjusted correlation for a certain value of MI is (Tsonis, 2001; Johnson and Wing, 2005; Osmane et al., 2022):

$$\rho_{adj} = \sqrt{1 - 2^{-2\mathrm{MI}}}. \tag{5}$$

Pearson correlation coefficient, ρ_P, is compared to the information adjusted correlation coefficient, ρ_{adj}, to study if the Pearson correlation coefficient underestimates the dependency of the variables because of the non-linear nature of the relationship. Similarly as done by Hoilijoki et al. (2022) we estimate the non-linearity as:

$$NL = 1 - \frac{|\rho_P|}{\rho_{adj}}. \tag{6}$$

In the case of the ρ_{adj} being larger than ρ_P, the non-linear statistical dependency between the two variables is significant and the non-linearity term *NL* increases. If ρ_{adj} is comparable to ρ_P , the non-linearity term *NL* is close to zero and there are no significant non-linear dependencies ie. system is nearly linear. The non-linearity defined here is similar to the one used by Tsonis (2001) and Johnson and Wing (2005), except for dividing the term by ρ_{adj} to get *NL* to vary between 0 and 1.

To estimate the reliability of the MI results we use surrogate data to quantify zero baseline for the MI values. We use randomly shuffled surrogates in this study. We calculate MI for 100 surrogates, calculate the average, MI_S, and standard deviation, σ_{MI}. If MI of for the original data is larger than $\mathrm{MI}_S + 3\sigma_{MI}$ the zero baseline, the MI value is considered significant. The calculated MI is significant in most of the cases because we use large amounts of data which leads to relatively small standard deviations.

https://doi.org/10.5194/angeo-2024-3
Preprint. Discussion started: 23 April 2024

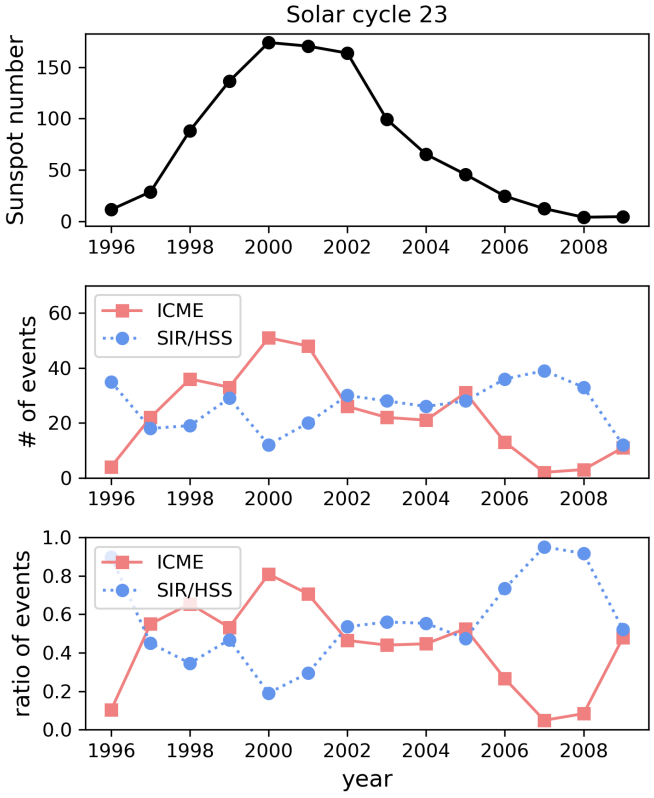

Figure 1. Top panel shows the sunspot number over the SC23. The middle panel shows the total number and bottom panel illustrates the ratio of ICMEs (pink) and SIRs/HSSs (blue) from all events driving geomagnetic activity during each year of the solar cycle.

3 Results

Solar cycle (SC) 23 covers the years from 1998 to 2008: solar maximum occurred between 1999-2002, declining phase 2003-2007, and minimum around 2008. The top panel of Figure 1 shows the yearly mean sunspot number (obtained from SILSO World Data Center (1996-2009) http://www.sidc.be/SILSO/) as the proxy of solar activity and the middle panel gives the number of ICMEs and SIR/HSS events counted from the data sets compiled by Richardson and Cane (2010) and Grandin et al. (2019), respectively. As the number of ICMEs and HSSs varies depending on the phase of the solar cycle, the ratio (bottom panel of Figure 1) of the type of the driver of geomagnetic storms also varies with solar activity levels. Most of the geomagnetic activity during solar maximum is driven by ICMEs while during the late declining phase the number of ICMEs decreases and almost all of the activity is caused by HSS and SIRs.

https://doi.org/10.5194/angeo-2024-3
Preprint. Discussion started: 23 April 2024

Annales Geophysicae Discussions

3.1 Impact of the phase of the solar cycle

To investigate the impact of the solar cycle on the correlation and non-linearity between solar wind and inner magnetosphere we calculate the correlation coefficients separately for each year between 1998 to 2008 during the SC23. We calculate the MI and ρ_P for different time offsets of the data sets with 1 h resolution for the range $0 - 169$ h and select the MI and ρ_P from the time offset that maximises the MI (in some occasions the MI and ρ_P are maximized at different time offsets). Using Equation 5 and 6 we compute the adjusted correlation and non-linearity, respectively. The solar wind parameters used in this study that are commonly accounted to be important in the solar wind–magnetosphere coupling are solar wind speed, V_{sw}, density, ρ, dynamic pressure, $P_{dyn} = \rho V_{sw}^2$, z-component of IMF, B_z, and $V_{sw}B_z = E_y$, which represents the solar wind electric field in the y direction (e.g. Vasyliunas, 1975) (e.g. Dungey, 1961; Newell et al., 2007; Wing et al., 2021). Here we use it as a simple approximation for the solar wind–magnetosphere coupling function, even though previous studies have shown that the system is more complicated and impacted by, for example, the magnetosheath (e.g. Borovsky and Birn, 2014). In addition to the solar wind parameters, we correlate AE index and SYM-H with the inner magnetospheric indices. The indices selected to describe the inner magnetosphere response are: the electron flux index F_{e130} for the 130 keV in the radiation belts describing the behaviour of the substorm injected seed electrons (Borovsky and Yakymenko, 2017) and the geosynchronous T_{geo} and ground-based T_{gr} Pc5 ULF wave indices.

The results from years 2001 and 2007 representing solar maximum and solar minimum, respectively, are shown in Figure 2. The top row shows color maps of the absolute value of the Pearson correlation coefficient $|\rho_P|$ between the solar wind (vertical axis) and inner magnetospheric parameters (horizontal axis) as well as AE and SYM-H indices, which are displayed on both axes. The second row shows ρ_{adj} calculated from MI and the non-linearity is displayed on the third row. The bottom panel g) illustrates the difference in the non-linearity terms in 2001 and 2007. In Figure 2 the white blocks indicate where the absolute value of the correlation coefficient is 0.3 or below i.e. correlation is weak or negligible.

The first column of each panel in Figure 2 is the electron flux index F_{e130}. The only solar wind parameters with larger than 0.3 Pearson correlation coefficient with the F_{e130} electron flux are the solar wind speed and density (the latter only in 2007). The linear correlations are significantly larger for the solar minimum year (panel 2d) than for the solar maximum year (panel 2a). The adjusted correlation ρ_{adj}, shown in panels b and e, shows moderate to strong correlation values between electron flux and all investigated solar wind parameters. The highest values are found for the solar wind speed and the values are again higher for the solar minimum year than for the maximum year. In 2007 the linear correlation is increased more than the adjusted correlation when compared to their 2001 values, and therefore, non-linearity (Figure 2c and f) is higher in 2001. The non-linearity is lowest for the solar wind speed compared to other solar wind parameters. In particular, this is evident for the solar maximum year 2001 for lower energy electron fluxes (F_{e130}). The high non-linearities between the rest of the solar wind parameters (ρ, P_{dyn}, B_z, and $V_{sw}B_z$) and F_{e130} are mainly due to the low Pearson correlation coefficient, although we note that ρ_{adj} is not that large either, suggesting that there are no significant statistical dependencies.

Figure 2g shows the difference between the non-linearity in 2001 and 2007. The positive values indicate larger non-linearity in 2001 and negative values show if the non-linearity was smaller in 2001. Majority of the parameter pairs studied show that

https://doi.org/10.5194/angeo-2024-3
Preprint. Discussion started: 23 April 2024

Annales Geophysicae Discussions
Open Access
EGU

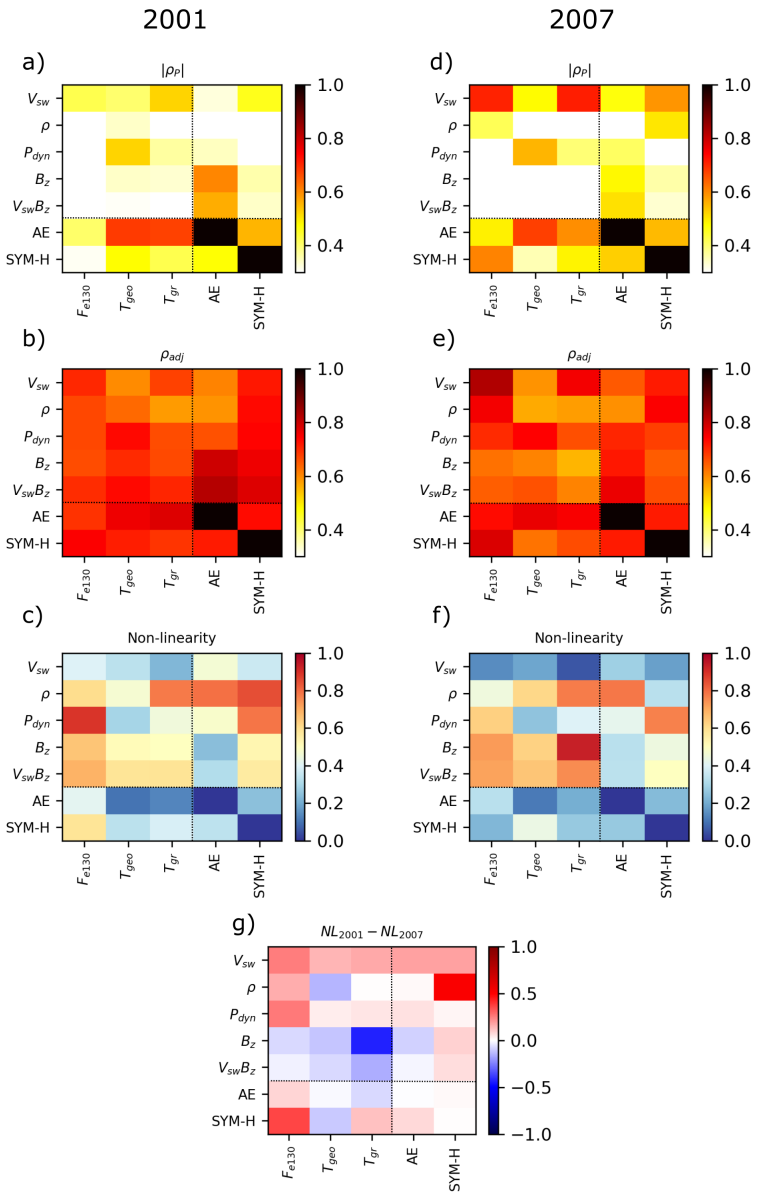

Figure 2. Absolute value of Pearson correlation coefficient, $|\rho_P|$, (top row), information adjusted correlation, ρ_{adj}, (second row), and non-linearity, $1 - |\rho_P|/\rho_{adj}$, (third row) between solar wind and inner magnetospheric variables and AE index and SYM-H in 2001 (left) and 2007 (right). Panel g) shows the difference between the non-linearity values between the two years. The dashed line divides the solar wind parameters (on the vertical axis) and the magnetospheric indices (on the horizontal axis) from the geomagnetic activity indices AE and SYM-H.

https://doi.org/10.5194/angeo-2024-3
Preprint. Discussion started: 23 April 2024

Annales Geophysicae Discussions
Open Access
EGU

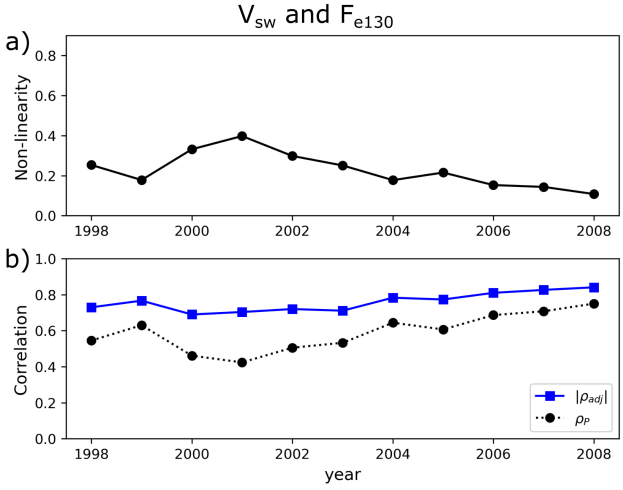

Figure 3. Non-linearity (top) and information adjusted correlation coefficient (ρ_{adj}) and Pearson correlation coefficient (ρ_P) for each year over SC23 between solar wind speed (V_{sw}) and 130 keV radiation belt electron flux index (F_{e130}) and V_{sw}.

the non-linearity was higher in 2001. Especially solar wind parameters V_{sw}, ρ and P_{dyn} have larger non-linearity during solar maximum than minimum. However, the parameter pairs that have solar wind B_z or $V_{sw}B_z$ as the solar wind driver show increase in non-linearity from solar maximum to minimum.

To illustrate further the variations in the non-linearity during the SC23 we plot the yearly correlation coefficients between V_{sw} and the outer radiation belt electron flux index. In Figure 3 the non-linearity (top panel a) and the correlation coefficients (bottom panels b) between the solar wind density and F_{e130} for 130 keV electrons. This figure shows that the adjusted correlation is higher than Pearson correlation coefficient at all times indicating that non-linearities are present through the solar cycle. The Pearson correlation coefficient ρ_P has its minimum at the solar maximum (2000-2001) and then increases towards the solar minimum. The adjusted correlation ρ_{adj} shows considerably smaller variations with solar activity levels which leads to non-linearity peaking during solar maximum.

Figure 2 also shows that out of the solar wind parameters, the geosynchronous Pc5 ULF wave index T_{geo} correlates the best with the dynamic pressure while the ground-based ULF wave index T_{gr} has the highest correlations (both for ρ_P and ρ_{adj}) with the solar wind speed. The non-linearity between P_{dyn} and T_{geo} is approximately the same (~ 0.3) at the solar maximum and minimum years (Figure 2c and f), therefore suggesting that their relationship does not significantly vary during solar cycle, while there is some decrease in the non-linearity between V_{sw} and T_{gr} from maximum to minimum. To explore this further in Figure 4a we plot the non-linearity between P_{dyn} and T_{geo} and in 4c between V_{sw} and T_{gr} across the SC23. The non-linearity between P_{dyn} and T_{geo} remains close to the same level throughout the whole solar cycle apart from a slight increase (~ 0.1) in 2003 during the early declining phase of the solar cycle. The non-linearity between V_{sw} and T_{gr} increases at solar maximum to ~ 0.2 and then decreases towards zero when the solar minimum approaches. The change is larger in the ρ_P but also ρ_{adj} increases slightly towards 2007.

https://doi.org/10.5194/angeo-2024-3
Preprint. Discussion started: 23 April 2024

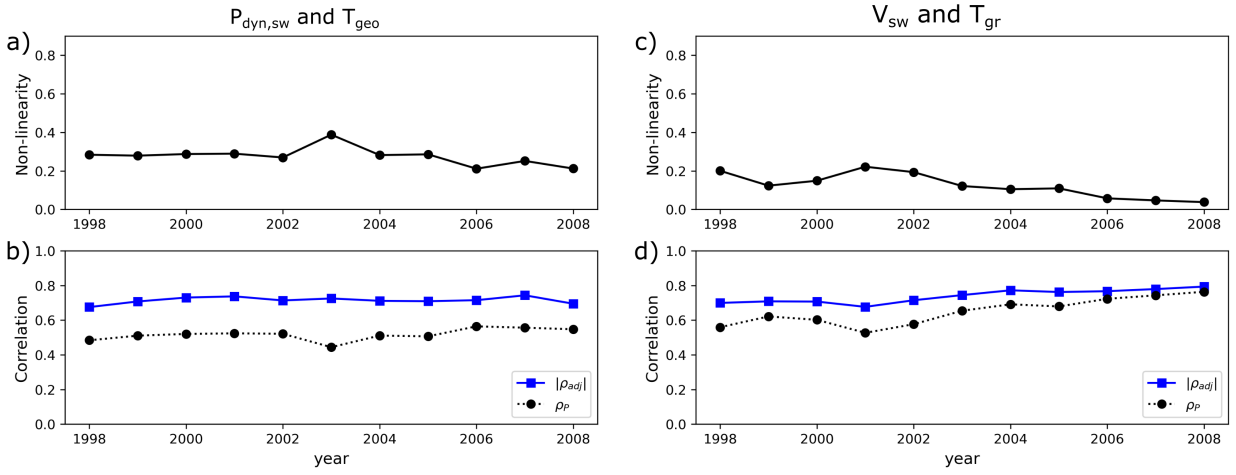

Figure 4. Non-linearity and information adjusted correlation, ρ_{adj}, and Pearson correlation coefficient, ρ_P, for each year over SC23 between $P_{dyn,sw}$ and T_{geo} (panels a and b) and V_{sw} and T_{gr} (panels c and d).

The solar wind parameter with the highest linear correlation coefficient with the AE index is B_z in 2001 (Figure 2a) and V_{sw} in 2007 (Figure 2d), while the highest non-linear correlation coefficient in both years with the AE index is the $V_{sw}B_z = E_y$ (Figure 2b and e). Both ρ_P and ρ_{adj} are slightly larger in 2001. To investigate the changes in the non-linearity over the solar cycle we plot it in Figure 5a. ρ_{adj} does not experience significant variation over the solar cycle, while ρ_P experiences considerable fluctuations, however, the changes have no clear solar activity trend. The non-linearity peaks in 2000 and in 2003 (~ 0.4). In solar maximum years, the ICME rate was the highest in 2000, although several prominent ICMEs in 2003 occurred that caused big geomagnetic storms such as the Halloween storm period. The SYM-H index has the highest linear correlation with the solar wind speed both in 2001 and 2007 (Figure 2a and d) but the non-linear correlation is highest with $V_{sw}B_z$ in 2001 and ρ in 2007.

Figure 2 shows that the relationship between AE index and the Pc5 ULF wave activity has low non-linearity during both the solar maximum and minimum and ρ_P and ρ_{adj} have quite similar values in each years. This is consistent with the results shown in Hoilijoki et al. (2022). Left and right panels of Figure 6 show the non-linearity and correlation coefficients between AE index and T_{geo} and T_{gr}, respectively. In all cases, the non-linearity remains low, and ρ_P and ρ_{adj} are approximately at the same level. The only notable trend is that ρ_P between AE and T_{gr} slightly decreases causing a small increase in the non-linearity towards the end of the SC23.

3.2 Impact of the driver of geomagnetic activity

The non-linearity between some solar wind parameters and inner magnetospheric indices, for example, V_{sw} and electron flux, shows dependence on the solar cycle. The number of ICMEs also closely follows the sunspot number as shown in Figure 1. This suggests that the number of ICMEs as the driver of the geomagnetic activity could be the cause of the increase in the

https://doi.org/10.5194/angeo-2024-3
Preprint. Discussion started: 23 April 2024

Annales Geophysicae Discussions
Open Access
EGU

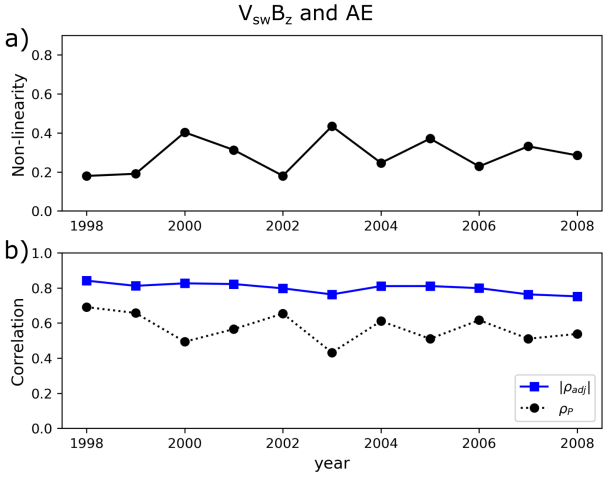

Figure 5. Non-linearity (a) and information adjusted correlation, ρ_{adj}, and Pearson correlation coefficient, ρ_P, (b) for each year over SC23 between $V_{sw}B_z$ and AE index.

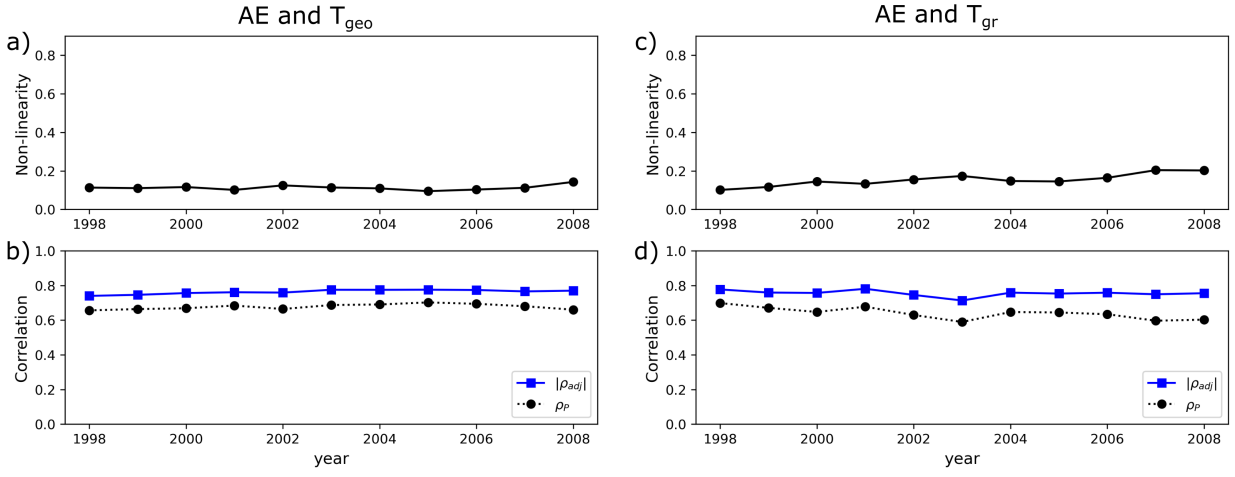

Figure 6. Non-linearity and information adjusted correlation, ρ_{adj}, and Pearson correlation coefficient, ρ_P, for each year over SC23 between AE index and T_{geo} (panels a and b) and AE index and T_{gr} (panels c and d).

https://doi.org/10.5194/angeo-2024-3
Preprint. Discussion started: 23 April 2024


Annales Geophysicae Discussions

non-linear dependency. To investigate this, we calculate the correlation coefficients separately for time periods of ICMEs (from Richardson and Cane list) and SIRs/HSSs (Grandin et al., 2019). In this study, the ICME time periods include also the preceding sheath regions and the HSS times include the SIR and the subsequent high speed stream. The remaining time periods are considered as quiet time solar wind, for which we account one day recovery time for the Earth's magnetosphere after the trailing edge of the ICME and HSS by excluding those recovery days from the correlation calculations. Using the ICMEs, SIRs/HSSs and quiet times from 1998 to 2008 we calculate the MI and correlation coefficients for the same solar wind parameters and inner magnetospheric indices as above. The left column of Figure 7 shows the results from the time periods of HSSs (a-c), the middle column (d-f) from ICMEs and the right column (g-i) from the quiet times.

The linear Pearson correlation coefficient between solar wind parameters and inner magnetospheric indices is higher during HSSs than ICMEs, and especially so for the V_{sw}, but the highest ρ_P between V_{sw} and electron flux index and ULF wave indices occurs during quiet time solar wind. In turn, linear correlations between the solar wind B_z and $V_{sw}B_z$ and AE index as well as geomagnetic activity indices (SYM-H and AE) and ULF wave indices are the highest during ICME events and lowest during the quiet solar wind. Depending on the parameter pair, ρ_{adj} may be highest during HSSs or ICMEs but in general the information adjusted correlation coefficient seems to be lowest during the quiet times apart from the solar wind speed that also has highest information adjusted correlation coefficients during the quiet solar wind time periods.

Solar wind dynamic pressure, IMF B_z and solar wind electric field $E_y = V_{sw}B_z$ have the lowest linear and non-linear correlation coefficients with the electron flux and ULF wave indices during all three event types but they are lowest during the quiet time. ρ_{adj} during the quiet time is low, which could be explained by the low activity in the inner magnetosphere as ULF waves are not excited. The values of the non-linearity are the highest for ICME-related periods. The higher linear correlation during SIR/HSSs leads to lower values of non-linearity compared to ICMEs (Figure 7a and d). This could be a result of SIR/HSS being less geoeffective than ICMEs especially during the late declining phase of SC23 (Zhang et al., 2008; Grandin et al., 2019). The non-linearity values during quiet times are generally between the values of HSSs and ICMEs or similar to HSS times except for the V_{sw} that has the most linear dependency between the electron flux and ULF wave indices.

4 Discussion

In this paper, we have investigated the solar cycle variations in the non-linear dependence between solar wind parameters and the inner magnetospheric indices. Non-linearity, *NL*, in this study is defined as the ratio of the linear Pearson correlation coefficient and information adjusted correlation (Equation 6). *NL* approaching 1 indicates that the correlation of the parameter pair is highly non-linear, while *NL* close to 0 indicates that the correlation is linear. Non-linearity between some of the solar wind - magnetosphere parameter pairs shows a clear dependence on the solar activity during the Solar Cycle 23 (SC23) while other parameter pairs do not.

The solar wind parameter having the strongest linear correlation with the inner magnetospheric parameters and indices, and especially with the electron fluxes, is the solar wind speed, as found in many previous studies (e.g. Paulikas and Blake, 1979; Baker et al., 1990; Li et al., 2005; Wing et al., 2016, 2021). We show here that the non-linearity is higher between

https://doi.org/10.5194/angeo-2024-3
Preprint. Discussion started: 23 April 2024

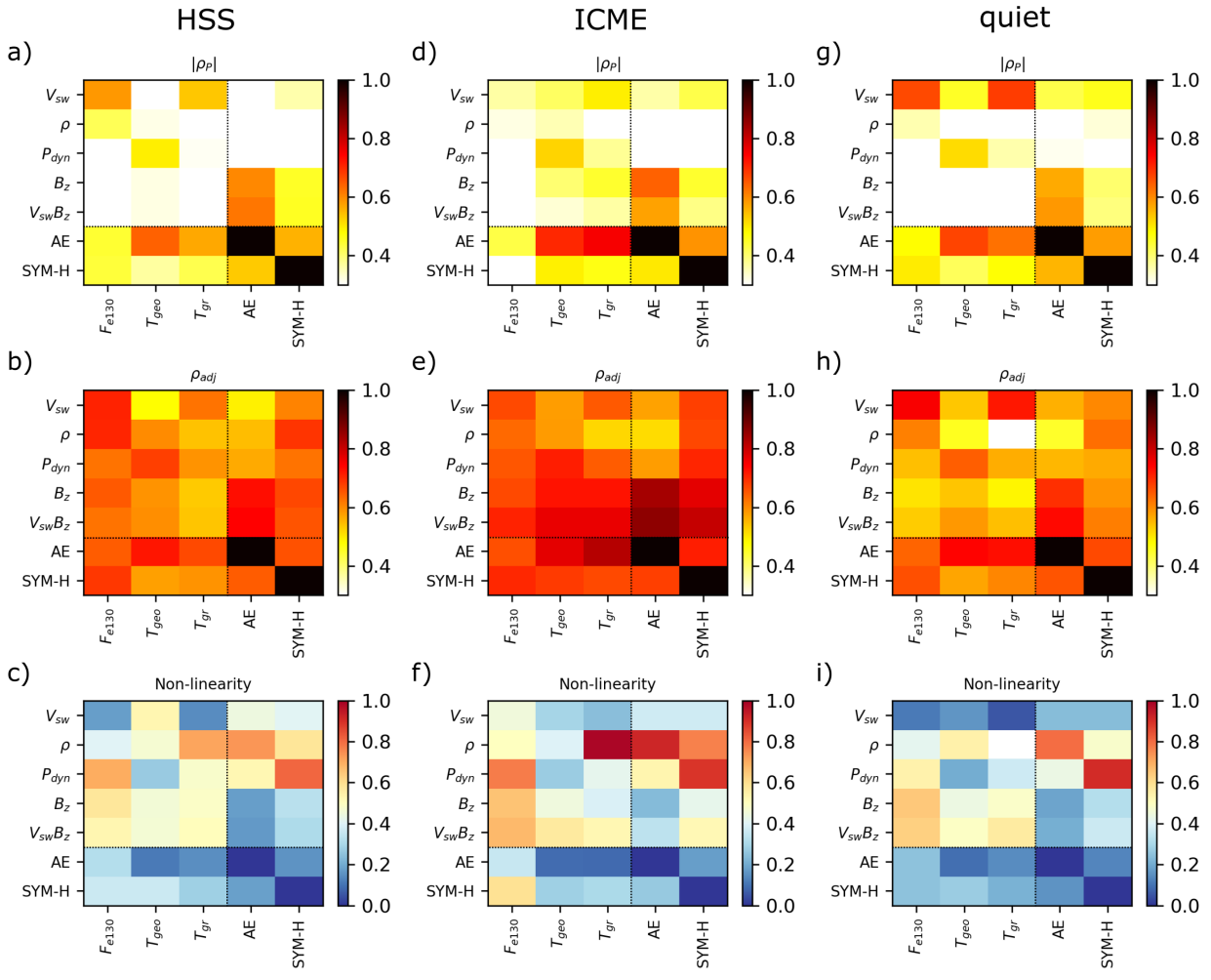

Figure 7. Pearson correlation coefficient, ρ_P, (top panels), information adjusted correlation, ρ_{adj}, (middle panels), and non-linearity ($1 - |\rho_P|/\rho_{adj}$), between solar wind and magnetospheric indices for time periods with HSSs (left column a–c), ICMEs (middle colums, d-f) and quiet time periods (right column g-i) between years 1998-2008. Dashed line divide the solar wind parameters (on the vertical axis) and the magnetospheric indices (on the horizontal axis) from the geomagnetic activity indices AE and SYM-H.

https://doi.org/10.5194/angeo-2024-3
Preprint. Discussion started: 23 April 2024

solar wind speed and outer radiation belt electron fluxes during solar maximum than during solar minimum. This behaviour quite closely follows the number of ICMEs as the driver of the geomagnetic activity as can be seen in Figure 3. Our results show that the correlation, both linear and non-linear, is larger during solar minimum than solar maximum. Investigating data separately for ICMEs and HSSs supports the conclusion that during the ICMEs the non-linearity is higher due to increased non-linear correlation and decreased linear correlation. ICME sheath regions have a dual effect on the radiation belts. On the other hand, their impact first typically deplete relativistic electrons from wide range of L-shells while the substorms during the sheath can refill the inner magnetosphere with seed energy electrons (e.g. Kalliokoski et al., 2020, 2023). The impact of the ICME ejecta following the sheath is highly dependent on its IMF B_Z profile. Southward IMF within the ejecta can lead to losses of radiation belt electrons across the magnetopause, as the more effective reconnection erodes the magnetopause closer to the Earth (George et al., 2020; George et al., 2022). In addition, the rotation profile of the magnetic field within the ejecta, south-north or north-south, can impact whether significant changes in the electron population occur during the leading or trailing boundary of the ejecta (George et al., 2020). SIRs also typically cause losses of relativistic electrons although to a smaller extent than ICME sheath regions (e.g. Turner et al., 2019). The fast streams following the SIRs tend to enhance the radiation belt electrons population up to relativistic energies especially if the the IMF is predominantly southward (e.g. Miyoshi et al., 2013). This is due to repeated substorms providing source and seed population to the inner magnetosphere and their progressive acceleration by chorus waves (e.g., Jaynes et al., 2015). The varying impact of the ICME ejecta (loss, enhancement or no-change) to radiation belt electrons of different energies is the likely cause of significant non-linearity in between the solar wind speed and electron fluxes at solar maximum years when the ICMEs are the most abundant. HSSs causing mainly enhancements or having only minor impact leads to higher linear correlation during the HSS driven activity that is dominant during the solar minimum years.

Unlike other studied solar wind parameters (speed, density, dynamic pressure), B_z and the solar wind electric field $E_y = V_{sw}B_z$ correlate with 130 keV electrons, ULF wave indices, and AE index more linearly during the solar maximum than the minimum. These results are consistent with a statistical study by Johnson and Wing (2005), who found that the K_p index and the solar wind driving as estimated using $V_{sw}B_S$ is more linear during solar maxima than during solar minima. Both B_z and E_y have the highest linear and non-linear correlations with the AE index, justifying that E_y has long been used as a simple proxy for the solar wind–magnetosphere coupling (e.g. Vasyliunas, 1975). Our results show that the statistical dependence between the simple coupling function, E_y, and AE is rather strong but their correlation is mostly non-linear. Both the linear and non-linear correlations are larger for the solar maximum in 2001 (Figure 2 and 5), even though the changes in the non-linearity do not follow as clearly the number of ICMEs as does the non-linearity between the solar wind speed and electron flux index. Dividing data to HSSs, ICMEs and quiet times shows also that during the most intense geomagnetic activity (i.e. during ICME driven activity), the correlation is the highest and during the quiet time solar wind the correlation is the weakest. Johnson and Wing (2005) concluded that the nonlinearity during the solar maximum is the lowest because the solar wind driving is strongest and, therefore, it suppresses the internal nonlinearities of the magnetosphere. This is consistent with our study in case for the IMF B_z and E_y but not for the other solar wind parameters. It could be that during stronger solar wind driving magnetosphere more directly responds to the magnetic field changes especially to IMF B_z via magnetic reconnection and likely suppressing

https://doi.org/10.5194/angeo-2024-3
Preprint. Discussion started: 23 April 2024


Annales Geophysicae Discussions

the impact of other solar wind parameters. This causes the non-linearity to increase for solar wind speed. On the other hand, during quiet solar activity the other solar wind parameters such as solar wind speed can have more direct impact on the inner magnetospheric dynamics though directly driving ULF Pc5 waves, for example, due to the Kelvin Helmholtz instability.

The strongest relationship between the T_{geo} and dynamic pressure and T_{gr} and solar wind speed highlight that the drivers of ULF waves at geosynchronous orbit and ground are partly different. This can be attributed to different drivers of different ULF wave modes and their propagation in the magnetosphere. The compressional and poloidal ULF modes are driven by internal sources and solar wind pressure fluctuations (e.g. Southwood et al., 1969), and as discussed in the Introduction, they do not propagate to the ground. The toroidal ULF modes in turn are able to reach to the ground, and are thus captured by the T_{gr} index. They are related to external drivers such as high solar wind speeds causing Kelvin-Helmholtz instability (e.g. Hudson et al., 2004; Claudepierre et al., 2008).

The ULF wave indices correlate strongly both linearly and non-linearly with the AE index, and therefore, the non-linearity is relatively low. Their relationship does not significantly vary over the solar cycle. The AE index describes quite well the substorm process and these results indicate that when the near-Earth magnetic field lines fluctuate in the Pc5 frequency range the substorm process is active. The ULF wave index could also be dominated by the substrorm driven fluctuations even though portion of the nightside MLTs (18-03) are excluded from the ground-based ULF wave index calculations.

5 Conclusions

This study highlights that the time period used in a statistical analysis can significantly impact the correlation coefficients even when using long periods (one year or more) of data. The obtained results show that under different overall solar activity conditions the response of the inner magnetosphere to certain solar wind parameters can differ. In case of solar wind speed, density and dynamic pressure, the solar wind –magnetosphere coupling becomes more non-linear during solar maximum than minimum and during ICMEs than HSSs or quiet solar wind periods. Especially, non-linearity between solar wind speed and 130keV electron flux index has a clear solar cycle trend, the correlation being considerably more linear during the solar minima. On the other hand, in case of solar wind IMF B_z and electric field $E_y = V_{sw}B_z$ the driving is more linear during the solar maximum than minimum. These could indicate that during stronger driving the increased magnetic field strength makes the inner magnetosphere response more linear to the changes in the magnetic field so that the magnetic reconnection process dominates the dynamics of the inner magnetosphere while suppressing the correlation between other solar wind parameters. Therefore, it is important to include the non-linear dependence between the different solar wind parameters and inner magnetosphere into the models predicting the solar wind–magnetosphere coupling, because the linear correlation coefficient does not reveal the whole story of the dependency of the the solar wind–magnetosphere coupling.

Data availability. Solar wind parameters and geomagnetic indices, AE and SYM-H, are obtained from NASA's OMNI data (https://omniweb.gsfc.nasa.gov/index.html). Source of sunspot numbers is WDC-SILSO, Royal Observatory of Belgium, Brussels (SILSO World Data Center,

https://doi.org/10.5194/angeo-2024-3
Preprint. Discussion started: 23 April 2024

1996-2009) (http://www.sidc.be/SILSO/). ULF wave indices are available at https://doi.org/10.2205/ULF-index (Pilipenko et al., 2017a). Data for the 1h electron flux index F_{e130} was calculated using data from SOPA instrument on board the LANL spacecraft by Borovsky and Yakymenko (2017) and can be requested from Joseph Borovsky. The code that was used to calculate the mutual information is publicly available on a GitHub repository (https://github.com/msavola/Mutual_information).

Author contributions. SH, EK and VL planned the study. VL found the changes in the non-linearity during solar cycle and SH carried out rest of the analysis and wrote the draft of the manuscript. MS wrote the analysis tools for calculating mutual information. All authors assisted with the interpretation of the results and reviewed the manuscript.

Competing interests. No competing interests

Acknowledgements. We acknowledge the Finnish Centre of Excellence in Research of Sustainable Space, Project 1336807, for supporting this research. The work of L. Turc is supported by the Research Council of Finland (UNTWINE project, Grant 322544).

https://doi.org/10.5194/angeo-2024-3
Preprint. Discussion started: 23 April 2024

Annales Geophysicae Discussions
Open Access
EGU

References

Baker, D. N., McPherron, R. L., Cayton, T. E., and Klebesadel, R. W.: Linear prediction filter analysis of relativistic electron properties at 6.6 RE, Journal of Geophysical Research: Space Physics, 95, 15 133–15 140, https://doi.org/10.1029/JA095iA09p15133, 1990.

Bentley, S. N., Watt, C. E. J., Owens, M. J., and Rae, I. J.: ULF Wave Activity in the Magnetosphere: Resolving Solar Wind Interdependencies to Identify Driving Mechanisms, Journal of Geophysical Research: Space Physics, 123, 2745–2771, https://doi.org/10.1002/2017JA024740, 2018.

Borovsky, J. E. and Birn, J.: The solar wind electric field does not control the dayside reconnection rate, Journal of Geophysical Research: Space Physics, 119, 751–760, https://doi.org/10.1002/2013JA019193, 2014.

Borovsky, J. E. and Denton, M. H.: Differences between CME-driven storms and CIR-driven storms, Journal of Geophysical Research: Space Physics, 111, https://doi.org/10.1029/2005JA011447, 2006.

Borovsky, J. E. and Yakymenko, K.: Systems science of the magnetosphere: Creating indices of substorm activity, of the substorm-injected electron population, and of the electron radiation belt, Journal of Geophysical Research: Space Physics, 122, 10,012–10,035, https://doi.org/10.1002/2017JA024250, 2017.

Claudepierre, S. G., Elkington, S. R., and Wiltberger, M.: Solar wind driving of magnetospheric ULF waves: Pulsations driven by velocity shear at the magnetopause, Journal of Geophysical Research (Space Physics), 113, A05218, https://doi.org/10.1029/2007JA012890, 2008.

Cover, T. M. and Thomas, J. A.: Elements of Information Theory Second Edition., John Wiley & Sons, Inc., Hoboken, New Jersey, 2006.

Dungey, J. W.: Interplanetary Magnetic Field and the Auroral Zones, Phys. Rev. Lett., 6, 47–48, https://doi.org/10.1103/PhysRevLett.6.47, 1961.

Elkington, S. R., Hudson, M. K., and Chan, A. A.: Acceleration of relativistic electrons via drift-resonant interaction with toroidal-mode Pc-5 ULF oscillations, Geophysical Research Letters, 26, 3273–3276, https://doi.org/10.1029/1999GL003659, 1999.

Elkington, S. R., Hudson, M. K., and Chan, A. A.: Resonant acceleration and diffusion of outer zone electrons in an asymmetric geomagnetic field, Journal of Geophysical Research (Space Physics), 108, 1116, https://doi.org/10.1029/2001JA009202, 2003.

George, H., Kilpua, E., Osmane, A., Asikainen, T., Kalliokoski, M. M. H., Rodger, C. J., Dubyagin, S., and Palmroth, M.: Outer Van Allen belt trapped and precipitating electron flux responses to two interplanetary magnetic clouds of opposite polarity, Annales Geophysicae, 38, 931–951, https://doi.org/10.5194/angeo-38-931-2020, 2020.

George, H., Reeves, G., Cunningham, G., Kalliokoski, M. M. H., Kilpua, E., Osmane, A., Henderson, M. G., Morley, S. K., Hoilijoki, S., and Palmroth, M.: Contributions to Loss Across the Magnetopause During an Electron Dropout Event, Journal of Geophysical Research: Space Physics, 127, e2022JA030 751, https://doi.org/10.1029/2022JA030751, e2022JA030751 2022JA030751, 2022.

Gonzalez, W. D., Joselyn, J. A., Kamide, Y., Kroehl, H. W., Rostoker, G., Tsurutani, B. T., and Vasyliunas, V. M.: What is a geomagnetic storm?, Journal of Geophysical Research: Space Physics, 99, 5771–5792, https://doi.org/10.1029/93JA02867, 1994.

Gonzalez, W. D., Tsurutani, B. T., and Clúa de Gonzalez, A. L.: Interplanetary origin of geomagnetic storms, Space Science Reviews, 88, 529–562, https://doi.org/10.1023/A:1005160129098, 1999.

Grandin, M., Aikio, A. T., and Kozlovsky, A.: Properties and Geoeffectiveness of Solar Wind High-Speed Streams and Stream Interaction Regions During Solar Cycles 23 and 24, Journal of Geophysical Research: Space Physics, 124, 3871–3892, https://doi.org/10.1029/2018JA026396, 2019.

https://doi.org/10.5194/angeo-2024-3
Preprint. Discussion started: 23 April 2024

Hoilijoki, S., Kilpua, E. K. J., Osmane, A., Kalliokoski, M. M. H., George, H., Savola, M., and Asikainen, T.: Using mutual information to investigate non-linear correlation between AE index, ULF Pc5 wave activity and electron precipitation, Frontiers in Astronomy and Space Sciences, 9, https://doi.org/10.3389/fspas.2022.987913, 2022.

Hudson, M. K., Denton, R. E., Lessard, M. R., Miftakhova, E. G., and Anderson, R. R.: A study of Pc-5 ULF oscillations, Annales Geophysicae, 22, 289–302, https://doi.org/10.5194/angeo-22-289-2004, 2004.

Hughes, W. J. and Southwood, D. J.: The screening of micropulsation signals by the atmosphere and ionosphere, Journal of Geophysical Research (1896-1977), 81, 3234–3240, https://doi.org/10.1029/JA081i019p03234, 1976.

Jaynes, A. N., Lessard, M. R., Takahashi, K., Ali, A. F., Malaspina, D. M., Michell, R. G., Spanswick, E. L., Baker, D. N., Blake, J. B., Cully, C., Donovan, E. F., Kletzing, C. A., Reeves, G. D., Samara, M., Spence, H. E., and Wygant, J. R.: Correlated Pc4–5 ULF waves, whistler-mode chorus, and pulsating aurora observed by the Van Allen Probes and ground-based systems, Journal of Geophysical Research: Space Physics, 120, 8749–8761, https://doi.org/10.1002/2015JA021380, 2015.

Johnson, J. R. and Wing, S.: A solar cycle dependence of nonlinearity in magnetospheric activity, Journal of Geophysical Research: Space Physics, 110, https://doi.org/doi.org/10.1029/2004JA010638, 2005.

Kalliokoski, M. M. H., Kilpua, E. K. J., Osmane, A., Turner, D. L., Jaynes, A. N., Turc, L., George, H., and Palmroth, M.: Outer radiation belt and inner magnetospheric response to sheath regions of coronal mass ejections: a statistical analysis, Annales Geophysicae, 38, 683–701, https://doi.org/10.5194/angeo-38-683-2020, 2020.

Kalliokoski, M. M. H., Henderson, M. G., Morley, S. K., Kilpua, E. K. J., Osmane, A., Olifer, L., Turner, D. L., Jaynes, A. N., George, H., Hoilijoki, S., Turc, L., and Palmroth, M.: Outer Radiation Belt Flux and Phase Space Density Response to Sheath Regions: Van Allen Probes and GPS Observations, Journal of Geophysical Research: Space Physics, 128, e2022JA030 708, https://doi.org/10.1029/2022JA030708, e2022JA030708 2022JA030708, 2023.

Kellerman, A. C. and Shprits, Y. Y.: On the influence of solar wind conditions on the outer-electron radiation belt, Journal of Geophysical Research: Space Physics, 117, https://doi.org/10.1029/2011JA017253, 2012.

Kilpua, E., Koskinen, H. E. J., and Pulkkinen, T. I.: Coronal mass ejections and their sheath regions in interplanetary space, Living Reviews in Solar Physics, 14, 5, https://doi.org/10.1007/s41116-017-0009-6, 2017a.

Kilpua, E. K. J., Balogh, A., von Steiger, R., and Liu, Y. D.: Geoeffective Properties of Solar Transients and Stream Interaction Regions, Space Science Review, 212, 1271–1314, https://doi.org/10.1007/s11214-017-0411-3, 2017b.

Kozyreva, O., Pilipenko, V., Engebretson, M., Yumoto, K., Watermann, J., and Romanova, N.: In search of a new ULF wave index: Comparison of Pc5 power with dynamics of geostationary relativistic electrons, Planetary and Space Science, 55, 755–769, https://doi.org/10.1016/j.pss.2006.03.013, ultra-Low Frequency Waves in the Magnetosphere, 2007.

Li, W.: Mutual information functions versus correlation functions, Journal of Statistical Physics, 60, 823–837, https://doi.org/10.1007/BF01025996, 1990.

Li, X., Baker, D. N., Temerin, M., Reeves, G., Friedel, R., and Shen, C.: Energetic electrons, 50 keV to 6 MeV, at geosynchronous orbit: Their responses to solar wind variations, Space Weather, 3, https://doi.org/10.1029/2004SW000105, 2005.

Mann, I. R., Lee, E. A., Claudepierre, S. G., Fennell, J. F., Degeling, A., Rae, I. J., Baker, D. N., Reeves, G. D., Spence, H. E., Ozeke, L. G., Rankin, R., Milling, D. K., Kale, A., Friedel, R. H. W., and Honary, F.: Discovery of the action of a geophysical synchrotron in the Earth's Van Allen radiation belts, Nature Communications, 4, 2795, https://doi.org/10.1038/ncomms3795, 2013.

https://doi.org/10.5194/angeo-2024-3
Preprint. Discussion started: 23 April 2024

Mann, I. R., Ozeke, L. G., Murphy, K. R., Claudepierre, S. G., Turner, D. L., Baker, D. N., Rae, I. J., Kale, A., Milling, D. K., Boyd, A. J., Spence, H. E., Reeves, G. D., Singer, H. J., Dimitrakoudis, S., Daglis, I. A., and Honary, F.: Explaining the dynamics of the ultra-relativistic third Van Allen radiation belt, Nature Physics, 12, 978–983, https://doi.org/10.1038/nphys3799, 2016.

March, T. K., Chapman, S. C., and Dendy, R. O.: Mutual information between geomagnetic indices and the solar wind as seen by WIND: Implications for propagation time estimates, Geophysical Research Letters, 32, https://doi.org/https://doi.org/10.1029/2004GL021677, 2005.

Mathie, R. A. and Mann, I. R.: On the solar wind control of Pc5 ULF pulsation power at mid-latitudes: Implications for MeV electron acceleration in the outer radiation belt, Journal of Geophysical Research: Space Physics, 106, 29 783–29 796, https://doi.org/10.1029/2001JA000002, 2001.

McPherron, R. L.: Magnetospheric substorms, Reviews of Geophysics, 17, 657–681, https://doi.org/10.1029/RG017i004p00657, 1979.

Miyoshi, Y., Kataoka, R., Kasahara, Y., Kumamoto, A., Nagai, T., and Thomsen, M. F.: High-speed solar wind with southward interplanetary magnetic field causes relativistic electron flux enhancement of the outer radiation belt via enhanced condition of whistler waves, Geophysical Research Letters, 40, 4520–4525, https://doi.org/10.1002/grl.50916, 2013.

Newell, P. T., Sotirelis, T., Liou, K., Meng, C.-I., and Rich, F. J.: A nearly universal solar wind-magnetosphere coupling function inferred from 10 magnetospheric state variables, Journal of Geophysical Research: Space Physics, 112, https://doi.org/10.1029/2006JA012015, 2007.

Osmane, A., Savola, M., Kilpua, E., Koskinen, H., Borovsky, J. E., and Kalliokoski, M.: Quantifying the non-linear dependence of energetic electron fluxes in the Earth's radiation belts with radial diffusion drivers, Annales Geophysicae, 40, 37–53, https://doi.org/10.5194/angeo-40-37-2022, 2022.

Osmane, A., Kilpua, E., George, H., Allanson, O., and Kalliokoski, M.: Radial Transport in the Earth's Radiation Belts: Linear, Quasi-linear, and Higher-order Processes, Astrophysical Journal, Supplement Series, 269, https://doi.org/10.3847/1538-4365/acff6a, 2023.

Paulikas, G. and Blake, J.: Effects of the Solar Wind on Magnetospheric Dynamics: Energetic Electrons at the Synchronous Orbit, pp. 180–202, American Geophysical Union (AGU), https://doi.org/10.1029/GM021p0180, 1979.

Pilipenko, V., Kozyreva, O., and Engebretson, M.: ULF wave index database, 10.2205/ULF-index, https://doi.org/10.2205/ULF-index, eSDB repository, GC RAS, Moscow, 2017a.

Pilipenko, V., Kozyreva, O., Engebretson, M., and Soloviev, A. A.: ULF wave power index for space weather and geophysical applications: A review, Russ. J. Earth Sci., 17, https://doi.org/https://doi.10.2205/2017ES000597, 2017b.

Pulkkinen, T.: Space Weather: Terrestrial Perspective, Living Reviews in Solar Physics, 4, 1, https://doi.org/10.12942/lrsp-2007-1, 2007.

Reeves, G. D., Morley, S. K., Friedel, R. H. W., Henderson, M. G., Cayton, T. E., Cunningham, G., Blake, J. B., Christensen, R. A., and Thomsen, D.: On the relationship between relativistic electron flux and solar wind velocity: Paulikas and Blake revisited, Journal of Geophysical Research: Space Physics, 116, https://doi.org/10.1029/2010JA015735, 2011.

Richardson, I. and Cane, H.: Near-Earth Interplanetary Coronal Mass Ejections Since January 1996, https://doi.org/10.7910/DVN/C2MHTH, 2024.

Richardson, I. G.: Solar wind stream interaction regions throughout the heliosphere, Living Reviews in Solar Physics, 15, 1, https://doi.org/10.1007/s41116-017-0011-z, 2018.

Richardson, I. G. and Cane, H. V.: Near-Earth Interplanetary Coronal Mass Ejections During Solar Cycle 23 (1996 - 2009): Catalog and Summary of Properties, Solar Physics, 264, 189–237, https://doi.org/10.1007/s11207-010-9568-6, 2010.

https://doi.org/10.5194/angeo-2024-3
Preprint. Discussion started: 23 April 2024

Richardson, Ian G. and Cane, Hilary V.: Solar wind drivers of geomagnetic storms during more than four solar cycles, J. Space Weather Space Clim., 2, A01, https://doi.org/10.1051/swsc/2012001, 2012.

Sarris, T. E., Li, X., Zhao, H., Papadakis, K., Liu, W., Tu, W., Angelopoulos, V., Glassmeier, K.-H., Miyoshi, Y., Matsuoka, A., Shinohara, I., and Imajo, S.: Distribution of ULF Wave Power in Magnetic Latitude and Local Time Using THEMIS and Arase Measurements, Journal of Geophysical Research: Space Physics, 127, e2022JA030 469, https://doi.org/10.1029/2022JA030469, e2022JA030469 2022JA030469, 2022.

Sheeley, N. R., J., Harvey, J. W., and Feldman, W. C.: Coronal holes, solar wind streams, and recurrent geomagnetic disturbances: 1973 1976, Solar Physics, 49, 271–278, https://doi.org/10.1007/BF00162451, 1976.

Shi, X., Baker, J. B. H., Ruohoniemi, J. M., Hartinger, M. D., Murphy, K. R., Rodriguez, J. V., Nishimura, Y., McWilliams, K. A., and Angelopoulos, V.: Long-Lasting Poloidal ULF Waves Observed by Multiple Satellites and High-Latitude SuperDARN Radars, Journal of Geophysical Research (Space Physics), 123, 8422–8438, https://doi.org/10.1029/2018JA026003, 2018.

Shprits, Y. Y., Elkington, S. R., Meredith, N. P., and Subbotin, D. A.: Review of modeling of losses and sources of relativistic electrons in the outer radiation belt I: Radial transport, Journal of Atmospheric and Solar-Terrestrial Physics, 70, 1679–1693, https://doi.org/10.1016/j.jastp.2008.06.008, 2008.

SILSO World Data Center: The International Sunspot Number, International Sunspot Number Monthly Bulletin and online catalogue, 1996-2009.

Simms, L. E., Engebretson, M. J., Rodger, C. J., Dimitrakoudis, S., Mann, I. R., and Chi, P. J.: The Combined Influence of Lower Band Chorus and ULF Waves on Radiation Belt Electron Fluxes at Individual L-Shells, Journal of Geophysical Research: Space Physics, 126, e2020JA028 755, https://doi.org/10.1029/2020JA028755, 2021.

Southwood, D., Dungey, J., and Etherington, R.: Bounce resonant interaction between pulsations and trapped particles, Planetary and Space Science, 17, 349–361, https://doi.org/https://doi.org/10.1016/0032-0633(69)90068-3, 1969.

Tsonis, A. A.: Probing the linearity and nonlinearity in the transitions of the atmospheric circulation, Nonlinear Processes in Geophysics, 8, 341–345, https://doi.org/10.5194/npg-8-341-2001, 2001.

Tsurutani, B. T., Gonzalez, W. D., Gonzalez, A. L. C., Guarnieri, F. L., Gopalswamy, N., Grande, M., Kamide, Y., Kasahara, Y., Lu, G., Mann, I., McPherron, R., Soraas, F., and Vasyliunas, V.: Corotating solar wind streams and recurrent geomagnetic activity: A review, Journal of Geophysical Research: Space Physics, 111, https://doi.org/10.1029/2005JA011273, 2006.

Turner, D. L., Kilpua, E. K. J., Hietala, H., Claudepierre, S. G., O'Brien, T. P., Fennell, J. F., Blake, J. B., Jaynes, A. N., Kanekal, S., Baker, D. N., Spence, H. E., Ripoll, J.-F., and Reeves, G. D.: The Response of Earth's Electron Radiation Belts to Geomagnetic Storms: Statistics From the Van Allen Probes Era Including Effects From Different Storm Drivers, Journal of Geophysical Research: Space Physics, 124, 1013–1034, https://doi.org/10.1029/2018JA026066, 2019.

Vasyliunas, V. M.: Theoretical models of magnetic field line merging, Reviews of Geophysics, 13, 303–336, https://doi.org/10.1029/RG013i001p00303, 1975.

Wing, S., Johnson, J. R., Camporeale, E., and Reeves, G. D.: Information theoretical approach to discovering solar wind drivers of the outer radiation belt, Journal of Geophysical Research: Space Physics, 121, 9378–9399, https://doi.org/10.1002/2016JA022711, 2016.

Wing, S., Johnson, J. R., Turner, D. L., Ukhorskiy, A., and Boyd, A. J.: Untangling the solar wind and magnetospheric drivers of the radiation belt electrons, Earth and Space Science Open Archive, p. 66, https://doi.org/10.1002/essoar.10508584.1, 2021.

https://doi.org/10.5194/angeo-2024-3
Preprint. Discussion started: 23 April 2024

Annales Geophysicae Discussions
Open Access
EGU

Zhang, Y., Sun, W., Feng, X. S., Deehr, C. S., Fry, C. D., and Dryer, M.: Statistical analysis of corotating interaction regions and their geoeffectiveness during solar cycle 23, Journal of Geophysical Research: Space Physics, 113, https://doi.org/10.1029/2008JA013095, 2008.